Polymer Degradation and Stability 124 (2016) 68–76

Contents lists available at ScienceDirect

Polymer Degradation and Stability

journal homepage: www.elsevier.com/locate/polydegstab

The effect of structure on thermal stability and anti-oxidation mechanism of silicone modified phenolic resin

Shan Li [a, b], Yue Han [a, b], Fenghua Chen [a], Zhenhua Luo [a], Hao Li [a, **], Tong Zhao [a, *]

[a] Laboratory of Advanced Polymer Materials, Institute of Chemistry, Chinese Academy of Sciences, Beijing 100190, PR China
[b] University of Chinese Academy of Sciences, Beijing 100049, PR China

ARTICLE INFO

Article history:
Received 4 November 2015
Received in revised form
11 December 2015
Accepted 16 December 2015
Available online 19 December 2015

Keywords:
Silane
Phenolic
Structure
Thermal stability
Anti-oxidation mechanism

ABSTRACT

In order to improve the thermal properties of the phenolic resin, silane with different degree of polymerization was introduced into phenolic resin by controllable reactions. Silicone phenolic resin was first synthesized via esterification reaction between methyltrimethoxysilane and novolac phenolic resin; then the degree of self-polymerization of silane was controlled by the hydrolyzation reaction. The designed structure of the hybrids was confirmed by Fourier Transform Infrared Spectroscopy (FTIR), Nuclear Magnetic Resonance (^{1}H-NMR and ^{29}Si-NMR), and curing of the hybrids was performed to obtain samples for microstructure observation and anti-oxidation evaluation. In situ self-polymerization of the silane during both the hydrolyzation and the curing processes led to phase separation in the cured hybrids, and the size of the phase structure increased with the increase of self-polymerization degree of the silane. Thermogravimetric analysis and high-temperature oxidation test were performed, and silane introduction was found to be beneficial to the enhancement of both thermal stability and oxidation resistance. Anti-oxidation mechanisms for the phenolic resin modified with silanes at different polymerization degree were compared and discussed.

1. Introduction

Phenolic is a class of thermosetting resin with excellent mechanical and thermal performances, and was widely used as matrix for thermal insulation, flame retardant and ablative materials [1–3]. However, its oxidation resistance at high temperatures needs to be further improved for the application in ablative and refractory materials [4,5]. Inorganic elements, such as boron [6–9], titanium [2,10] and silicon [1] were found to exhibit excellent oxidation resistance, and have been successfully introduced into to phenolic resin (PR), enhancing its oxidation performance.

The merit of organic silicone is their attractive integrated properties including thermal stability [11,12], flame retardancy [13], toughness [14] and moisture resistance [15]. It is of great interest to introduce silicone into organic polymers [16–20] to endow the hybrids with excellent properties from both components. Many studies proved that silicone is an effective component in improving the anti-oxidation properties of polymers [12,17,20,21]. K. Haraguchi and co-workers [21,22] prepared phenolic/silica hybrid by in-situ polymerization of silicon alkoxide, and both mechanical and thermal properties were enhanced. Silicone and phenolic resin were incompatible, and phase separation would always occur in the hybrids [12,23,24]. The phase structure (including dispersion state [25], particle size [14,26] and interface of the phases [21]) would affect the properties of the hybrids.

Microstructure was responsible for the properties, and its relationship with mechanical properties was intensively studied. Unfortunately, less effort was made on the effect of microstructure on the thermal properties. Yong Nie et al. [16] claimed that the epoxy dispersed with nanoscale polyhedral oligomeric silsesquioxane (POSS) cages has better anti-oxidation properties than that possessing microscale separated phase structures. Researchers have revealed that the anti-oxidation mechanism is complicated and greatly depended on the microstructure (including interfaces [27,28], holes and cracks [29,30], etc) and chemical structure [31,32] of the materials. As far as we knew, such understanding for silicone modified phenolic system was rarely reported, which would benefit the structure design of anti-oxidative silicone modified phenolic resin.

To obtain different phase structure, the control of polymerization degree of the silane in phenolic resin may be an effective

* Corresponding author.
** Corresponding author.
E-mail addresses: lihao306@iccas.ac.cn (H. Li), tzhao@iccas.ac.cn (T. Zhao).

http://dx.doi.org/10.1016/j.polymdegradstab.2015.12.010
0141-3910/

method [33,34]. Here in this report, we controlled the ratio between grafted and self-polymerized silane within silicone phenolic resin by a two-step synthesis process. Silicone phenolic resin was first synthesized via esterification reaction between methyltrimethoxysilane and novolac phenolic resin, then the degree of self-polymerization of silane was controlled by the hydrolyzation reaction. The in situ self-polymerization of silane in hybrids led to the changing of the structure and morphology. The thermal stability and oxidation resistance of silicone phenolic resin was studied by thermogravimetric analysis and high-temperature oxidation test. The anti-oxidation mechanism for the hybrids with different structures was proposed and discussed.

2. Experimental

2.1. Materials

Novolac phenolic resin (PF-8013) was supplied by Shandong Jinan Shengquan Co. Ltd, China. Methyltrimethoxysilane was purchased from Hubei New Blue Co. Ltd, China. Acetic acid was purchased from Beijing Chemical Works, and hexamethylene tetramine (HMTA), the curing agent for the novolac resin and hybrids, was obtained from Sinopharm Chemical Reagent Co. Ltd.

2.2. Preparation of the hybrid resin

2.2.1. Synthesis of the silicone modified novolac phenolic resin (SN)

SN was synthesized in a 250 mL three-neck round-bottom flask reactor equipped with a thermometer, a stirrer, and a reflux condenser. Novolac phenolic resin (NR) (103.3 g), methyltrimethoxysilane (136.0 g), and acetic acid (1.03 g) were stirred and gradually heated to 100 °C, and then kept heating for 20 h. At the end of the reaction, the unreacted methyltrimethoxysilane and byproducts were distilled under reduced pressure at 130 °C for 40 min, and then SN was obtained. The synthesis route for SN is shown in Scheme 1.

2.2.2. Hydrolyzation and condensation reaction of SN

Different amount of water was added to the SN ethanol solutions, and refluxed at 80 °C for 10 h. At the end of the reaction, the resin was distilled under reduced pressure at 100 °C to remove the byproducts and solvent. The reaction rout is shown in Scheme 2. The water amount was 2 wt%, 6 wt%, 10 wt% of SN and the obtained hybrid resin was designated as SN-2%H_2O, SN-6%H_2O SN-10%H_2O, respectively.

2.2.3. Preparation of cured specimens

The curing agent, HMTA, was then added into the hybrid ethanol solutions with a loading level of 10 per hundred ratio of the hybrids by weight. The solvent was removed at room temperature under vacuum to get hybrid resins containing curing agent. The samples were cured following the procedure 80 °C (4 h) +120 °C (2 h) +180 °C (4 h).

2.3. Measurements

Fourier Transform Infrared Spectroscopy (FTIR) measurements were performed on a Tensor-27 spectrometer at room temperature. Samples were grinded, mixed with KBr and pressed into small flakes for testing. ^{1}H-NMR and ^{29}Si-NMR spectra were recorded on a Bruker Avance 400 MHz NMR spectrophotometer. Thermolgravimetric analysis (TGA) was carried out from ambient temperature to 900 °C on a Netzsch STA409PC at a heating rate of 10 °C min^{-1} in nitrogen and air atmosphere, respectively. The samples were quenched and cracked in liquid nitrogen, and fracture surface of the hybrids was observed on a Hitachi S-4800 scanning electron microscope (SEM) at an accelerating voltage of 10 kV. Energy dispersive X-ray spectroscopy (EDX) was performed on an Oxford INCAx-sight 7593 system attaching to the SEM apparatus. High-temperature oxidation test was performed in a muffle furnace; the furnace was heated to the desired temperature before the powdered samples were put into the furnace and kept for 30 min. X-ray photoelectron spectroscopy (XPS) measurement was performed using an ESCALAB250XI instrument. The Raman spectra were recorded on a Renishaw inVia plus using the 633 nm excitation line of an Argon-ion laser.

3. Results and discussion

3.1. Structure characterization of the hybrids

FTIR and NMR were used to characterize the structure of hybrid resins, and the spectra were shown in Fig. 1 and Fig. 2. It can be seen that Si–O–ph signals at 949 cm^{-1} was formed after the esterification reaction between novolac and methyltrimethoxysilane. With the amount of water increasing, the signal intensity at 949 cm^{-1} (ascribed to Si–O–ph) became weak, while the peak intensity at 1057 cm^{-1} (corresponding to Si–O–Si vibration [17]) became stronger. The decreased Si–O–ph signal revealed that the Si–O–ph was not stable and would decompose to a certain extent after the hydrolyzation reaction; the breaking down of Si–O–ph would weaken the interactions between silane and phenolic. The increased Si–O–Si signal suggested the self-condensation of silane. According to ^{1}H NMR shown in Fig. 2, the integral ratio (R) between the proton signals of Si–OCH_3 and that of –CH_2– decreased with the increase of water content, which further confirmed the hydrolyzation and condensation reaction of Si–OCH_3. The degree of both breaking down of Si–O–ph and polycondensation of Si–OCH_3 could be controlled by varying the amount of water. The bulk samples of SN and SN-2%H_2O were both transparent; the SN-6%H_2O was translucent, and the SN-10%H_2O was opaque, which might be related to phase separations within the hydrolyzed hybrids [22].

The ^{29}Si-NMR spectrum was displayed in Fig. 3. The signal at –45 ppm was attributed to the Si–O–phenyl, suggesting that most MTMS was grafted onto the phenol groups of phenolic resin in the first reaction. When 2 wt% water was added, the intensity of the signal for Si–O–ph decreased and new signals at –57 and –66 ppm appeared, which corresponded to T_2 and T_3 groups, respectively [35,36], as shown in Scheme 2. It further confirmed that the

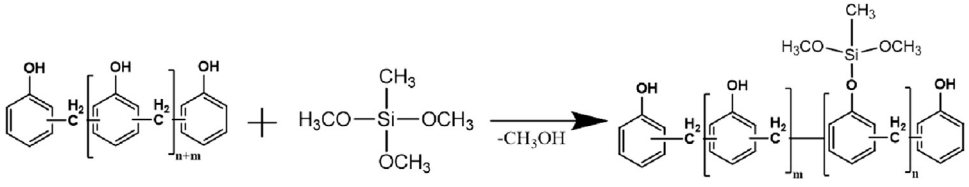

Scheme 1. The synthesis reaction for SN.

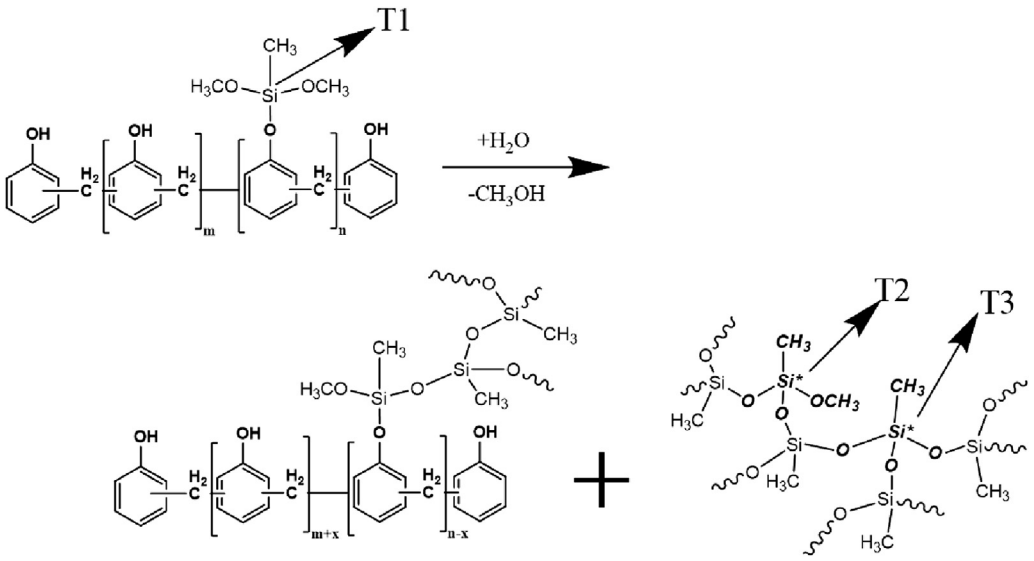

Scheme 2. The hydrolysis and condensation reaction of SN.

hydrolyzation reaction of the SN not only broke the Si–O–ph but also led Si–OCH_3 to hydrolyze and condense, forming pre-polymerized silicone resin, as shown in Scheme 2. With the water amount increasing, the peak intensity of T_1 decreased while that of T_2 and T_3 increased, which was consistent with the FTIR and ^{1}H-NMR analysis.

3.2. Structure and morphology of the cured hybrids

FTIR and Solid ^{29}Si-NMR characterizations were performed to study the chemical structure of the cured hybrids. As shown in Fig. 4a, after curing the signal of Si–O–ph still existed, and the intensity decreased with the water content increasing, and it was very weak in cured SN-10%H_2O. Fig. 4b shows that in cured SN, T_1 structure vanished, while signals at −54 ppm and −61 ppm (corresponding to silicone intermediate [37]) increased. For cured hybrids after hydrolyzation, T_1 signals completely disappeared, and the integral ratio between signals of T_3 and T_2 increased with the water content increasing, suggesting that the silane was more condensed in higher amount of water after curing. The above analysis revealed that silane in both the SN and the hydrolyzed SN could be further polycondensed during curing and chemical bond between silane and phenolic still existed after curing.

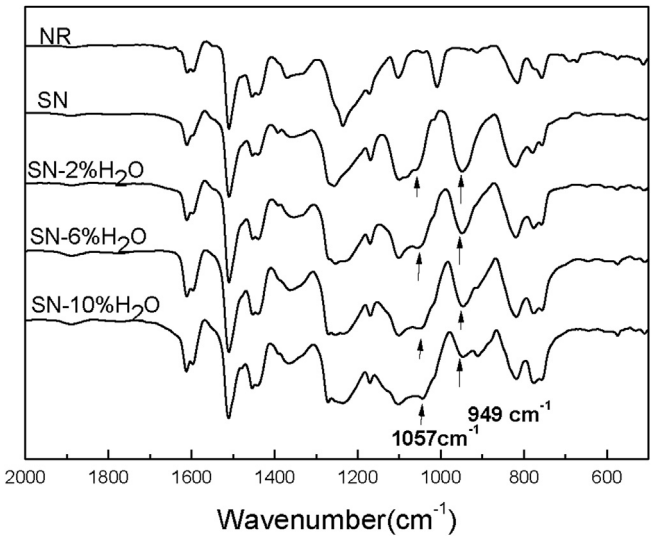

Fig. 1. FTIR of the hybrids hydrolyzed with different amount of water.

The fracture surface of the cured resin was characterized by SEM, and the corresponding images were shown in Fig. 5. The surface of cured SN was smooth and no micro-phase separation was observed. The cured SN-2%H_2O presented "sea-island" morphology with particles size of about 200 nm, and blurred interface. For cured SN-6%H_2O, the particle size grew to about 500 nm, while maintaining the blurred interface. The cured SN-10%H_2O showed a larger particle size (about 2–3 μm) and clear interfaces, suggesting weakening of the interfacial interactions between the silicone rich phase particles and phenolic matrix [24].

The different morphology was associated to the chemical structure of the hybrids. For SN, the silane monomer was mostly grafted on the phenol groups and its self-condensation degree was low after curing; so the hybrid remained transparent and homogenous. The very small amount of water formed during curing did not have obvious effects on the morphology of SN. When the SN was hydrolyzed, the Si–O–ph was broken, and the Si–OCH_3 was hydrolyzed and self-condensed; resulting in a decrease in the mixing enthalpy between the two components, and further aggregation of the silicone during curing, thus forming silicone resin rich domains in the phenolic matrix. At low water amount, not all of the Si–O–ph was broken, and hydrolyzation-condensation of the Si–OCH_3 was not complete. The remained Si–O–ph generated strong interactions between the phenolic and silicone rich domains, resulting in the blurred interface in Fig. 5b,c. In SN-10%H_2O, most of the Si–O–ph was broken, larger aggregated particles and clear interface were formed due to the reduced miscibility and the further condensed silicone rich domains.

3.3. Thermal degradation behavior

TGA measurements were employed to investigate the thermal stability of the cured hybrids. In N_2 atmosphere (as shown in Fig. 6a), the initial thermal degradation temperature ($T_{5\%}$) of the cured SN increased from 390.1 °C (that of NR) to 411.6 °C. For cured SN-2%H_2O, the $T_{5\%}$ decreased when compared with cured SN. The decrease was attributed to the volatilization of incompletely cured

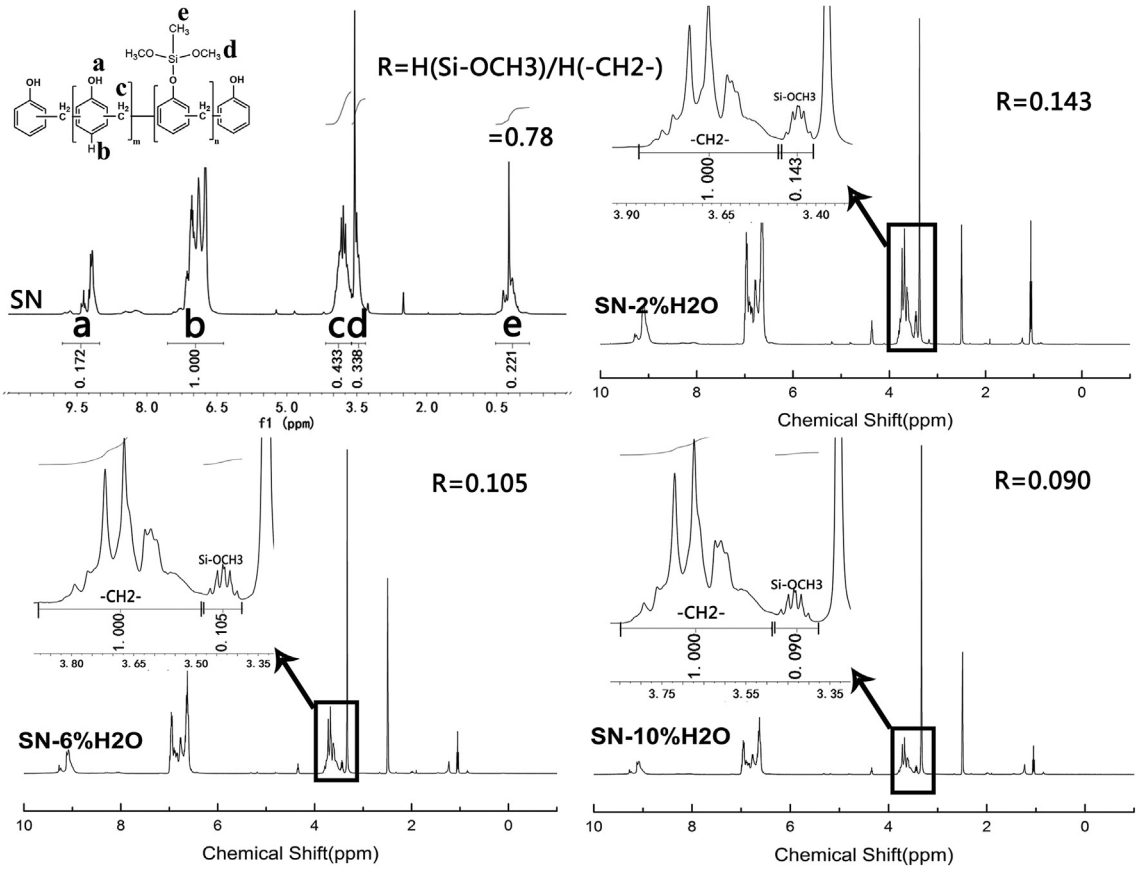

Fig. 2. 1H-NMR of the hybrids hydrolyzed with different amount of water.

silicone prepolymers, which may be generated from the hydrolyzation-condensation reaction at insufficient water content (2%H_2O). With the water amount increasing, the $T_{5\%}$ did not change significantly. From the DTG curves (shown in Fig. 6b), it can be clearly seen that the decomposition peak temperature ($T_{d,max}$) of SN was higher and the decomposition rate was lower, suggesting that silane grafted on phenolic could effectively protect the matrix from degradation. Given with insufficient water (2%H_2O), the curing of the silicone group was incomplete, resulting a higher decomposition rate. The proper amount of water could ensure the complete curing of the silicone group and the formation of strong interfacial interactions between the two phases; hence the decomposition rate was similar as SN and the $T_{d,max}$ was even higher. On the contrary, when excess water was provided, the silicone phase was separated from the main phenolic phase; the formed clear interface would accelerate the decomposition reaction.

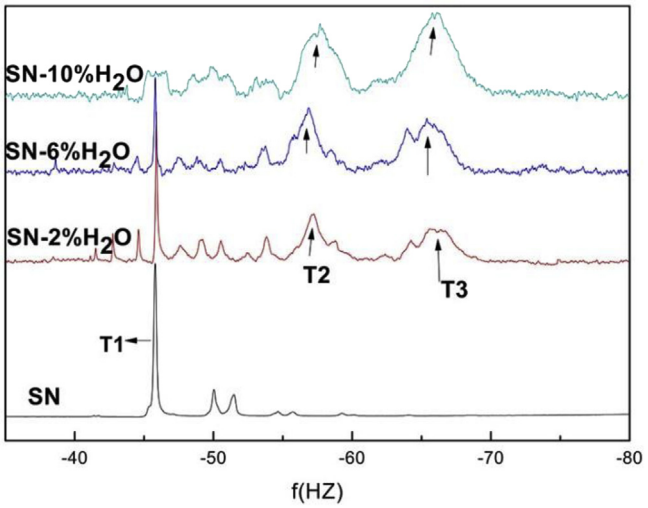

Fig. 3. ^{29}Si NMR of the hybrids hydrolyzed with different amount of water.

In air, the trend of the initial decomposition temperature of different hybrids was similar as that in N_2 atmosphere. The residual weight of cured NR is null. With the amount of water increasing, the residual weight at 900 °C (R_{900}) increased, suggesting that the higher polymerization degree of the silicone domains in phenolic matrix accounted for the higher residual after high temperature oxidation. This was confirmed in the following analysis. SN has higher $T_{d,max}$, but the residual weight was too low, which was only 6.18%. For SN-6%H_2O, the R_{900} was increased to 13.98%.

High temperature oxidation test was conducted in muffle furnace to investigate the weight retention of the hybrids oxidized at different temperatures. The powdered samples of the hybrids were treated at 500, 600, 700, 800, 900, 1000 °C for 30 min respectively. The weight retention was calculated from the differences in sample weight before and after the oxidation, and the results were displayed in Fig. 7. After treated at 500 °C for 30 min, the weight retention was similar among different hybrids, about 82.5%. The weight residual was significantly decreased after treated at 600 °C for 30 min, suggesting that the hybrids decomposed rapidly at 600 °C, which was in good consistence with the TGA results. At higher temperatures the weight retention decreased but

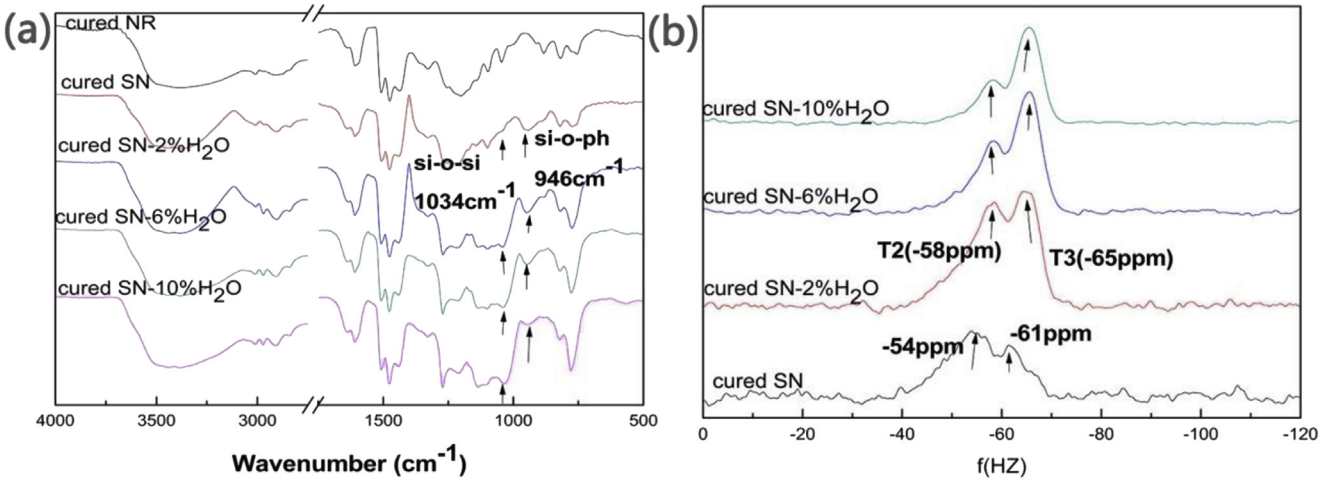

Fig. 4. (a) FTIR and (b) Solid ^{29}Si-NMR of the cured hybrids.

did not change dramatically. It was clear that the SN-2%H_2O had the lowest weight retention and the other hybrids exhibited slightly higher residual weight than NR.

3.4. Structure of the oxidized resin

3.4.1. Microstructure of the oxidized resin

For understanding the anti-oxidation mechanism of the hybrid with different morphology, microstructure and chemical structure of the oxidized resin were characterized. Microstructure of the oxidized hybrid (1000 °C for 30 min) was observed by SEM (as shown in Fig. 8). The homogenous SN was still compact with only a few holes and cracks appearing on the surface, which were the channels for the gas releasing. In oxidized SN-2%H_2O, the dispersed phase was no longer as compact as that in cured hybrid, and many small holes were generated in the dispersed particles as shown in the inset in Fig. 8b. SN-6%H_2O, after oxidation, the contrast between the dispersed phase and the matrix became higher, and the silicone-rich domains were well preserved. This phenomenon became more predominant in SN-10%H_2O, whose interface became sharp and clear.

3.4.2. Chemical structure of the oxidized resin

To further elucidate the anti-oxidation mechanism of hybrids with different chemical structures, SN and SN-6%H_2O were taken as examples and characterized by FTIR, Raman, EDX and XPS. FTIR was performed on the hybrids oxidized at different temperatures, and the corresponding spectra were shown in Fig. 9. After oxidation at 500 °C for 30 min, both samples exhibited phenolic hydroxyls (at 1212 cm^{-1}) and methylene (at 1468 cm^{-1}) signals. However, after oxidation at 600 °C for 30 min, the organic groups almost disappeared, which was in accordance with the severe weight loss at

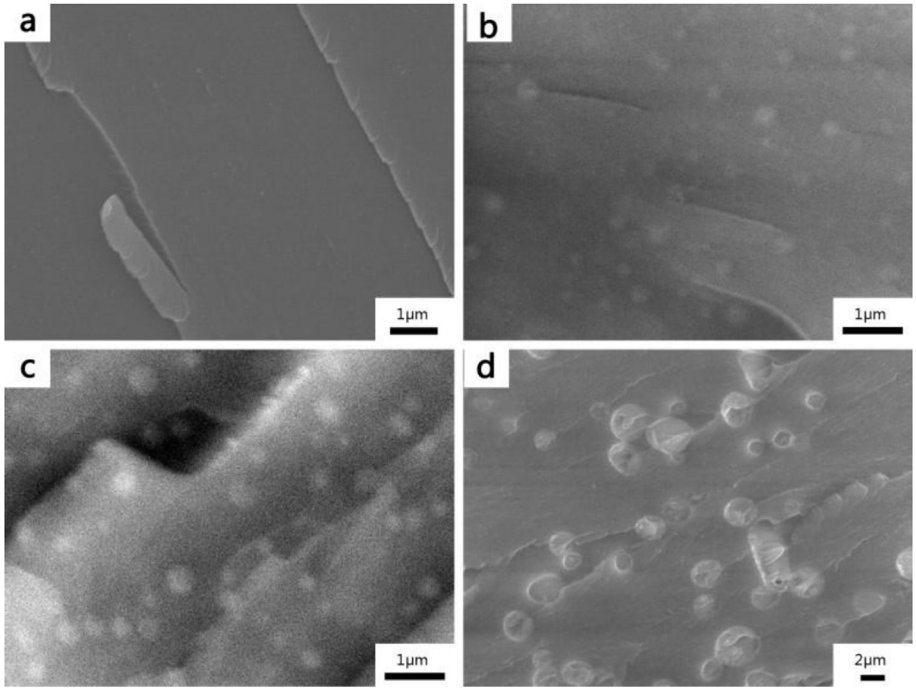

Fig. 5. SEM images of the cured hybrids (a) SN (b) SN-2%H_2O (c) SN-6%H_2O (d) SN-10%H_2O.

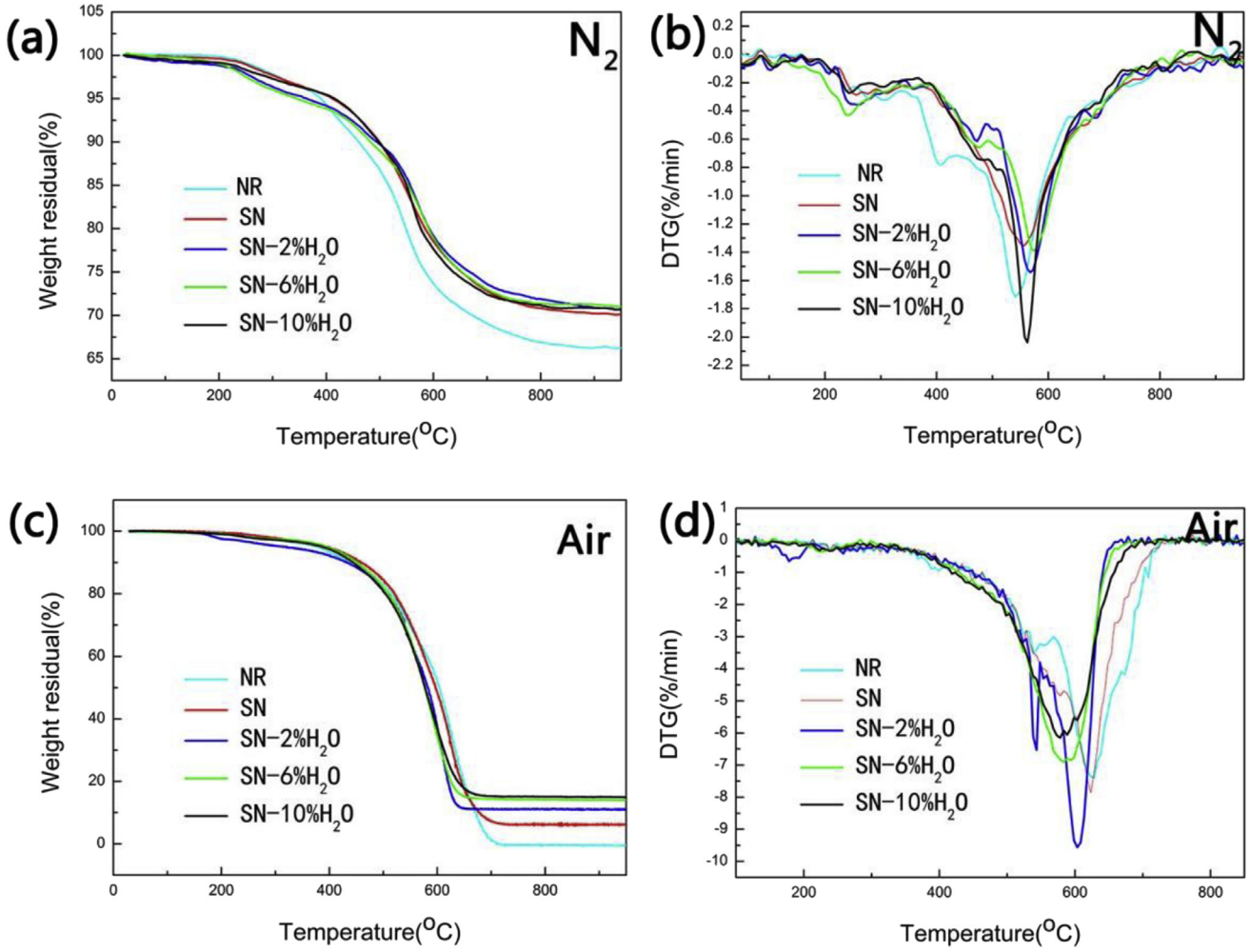

Fig. 6. TGA curves of cured NR, SN and SN with different amount of water: (a) (c) Residual weight–temperature curves; (b) (d) Derivative thermogravimetric curves (DTG).

600 °C shown in Fig. 7. After higher temperature (800, 1000 °C) oxidation, the peak at 1098 cm^{-1} (attributed to Si–O–Si) in the spectrum of SN significantly decreased, suggesting that the Si–O bond was broken to some extent. In the spectrum of SN-6%H_2O, the peak at 1098 cm^{-1} was obvious even after oxidation at 1000 °C for 30 min, indicating that the Si–O–Si was well preserved during high temperature oxidation.

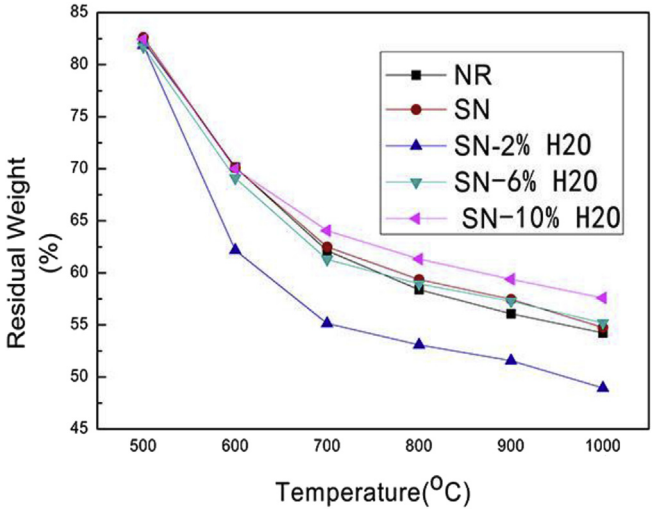

Fig. 7. The weight retention of the cured hybrids after oxidation at different high temperatures.

EDX (shown in Fig. 10) was employed to study the element content and distribution within the samples. The silicon content was about 6.38%, 6.87% in the cured SN and SN-6%H_2O, respectively. After oxidation at 1000 °C for 30 min, the silicon was evenly distributed within the oxidized SN, as shown in Fig. 10c. The weight retention was about 54% after oxidization at 1000 °C for 30 min (shown in Fig. 6), thus the silicon content in the oxidized resin should be 11.8% theoretically. Actually, the silicon content was about 7.24%, much lower than the theoretical amount, revealing that some silicone-containing structures lost during the high temperature oxidation. In oxidized SN-6%H_2O, silicon element mainly aggregated in the particles (as shown in Fig. 10f), and the silicon content was 11.60%, much higher than that in oxidized SN, revealing that silicone-containing structures were mostly preserved after the high temperature oxidation.

XPS was used to study the chemical states of silicon and oxygen atoms in the oxidized resin. The spectra were shown in Fig. 11, in which oxygen and silicon peaks were observed in the full scan spectrum. High resolution Si_{2p} peak was separated, and signals at 103.2 eV and 102.4 eV, corresponding to SiO_2 and Si–O structures respectively, could be found. Silicone in the form of SiO_2 (at 103 eV)

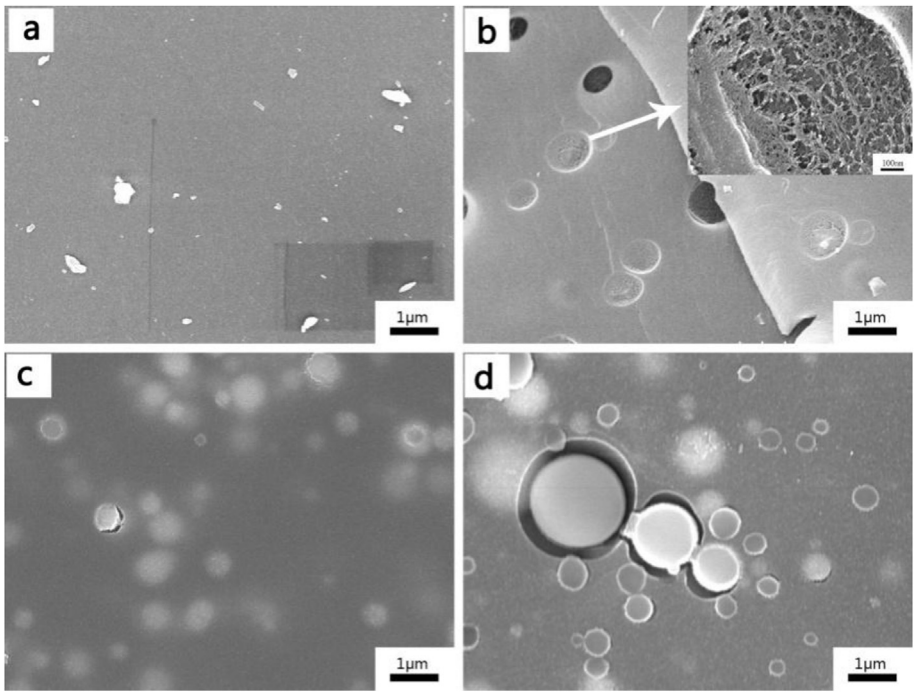

Fig. 8. SEM images of the hybrids after 1000 °C oxidation (a) SN (b) SN-2%H_2O (c) SN-6%H_2O (d) SN-10%H_2O.

in oxidized SN-6%H_2O was much higher than that in oxidized SN. O1 peak at 533.2 eV, O_2 peak at 532.5 eV and O3 peak at 531.8 eV separated from the O1s spectrum could be assigned to the C–O–, Si–O– and C–OH, respectively. In oxidized SN-6%H_2O, the peak intensity of oxygen in the form of Si–O– was higher than that of oxidized SN, while the C–O peak intensity was lower. The higher amount of silicon in the form of SiO_2 in oxidized SN-6%H_2O revealed that silicon in SN-6%H_2O could consume permeated oxygen during oxidation [38]; while in SN, oxygen was mainly consumed by carbon.

The Raman spectra of the hybrids after oxidation at 1000 °C for 30 min were displayed in Fig. 12. Carbon materials typically exhibit two broad bands in the Raman spectra. The D band at 1350–1380 cm^{-1} attributes to disordered turbostratic structures, while the G band at 1580–1600 cm^{-1} is assigned to the ordered graphitic structures. The intensity ratio of two bands (I_D/I_G) could reflect the order of carbon [39,40]. A lower I_D/I_G value indicates higher graphitization degree of carbonaceous materials [41]. As seen in Fig. 12, all spectra exhibited two typical distinct bands for the carbonized hybrids. Compared with NR char, SN and SN-10% H_2O char have a lower I_D/I_G value. The results indicated that the presence of silicon atom in the network did not disrupt the formation of graphene sheet, and was able to promote graphitization of NR at high temperatures. The thermal properties of hybrids may also be attributed to the formation of more orderly carbon structure [42].

The anti-oxidation mechanism was depicted as following. For SN, the silane grafted on the phenolic resin could protect the phenol groups from oxidation, thus the $T_{d.max}$ was higher. However, the grafted silane was incompletely cured (as illustrated in Fig. 4),

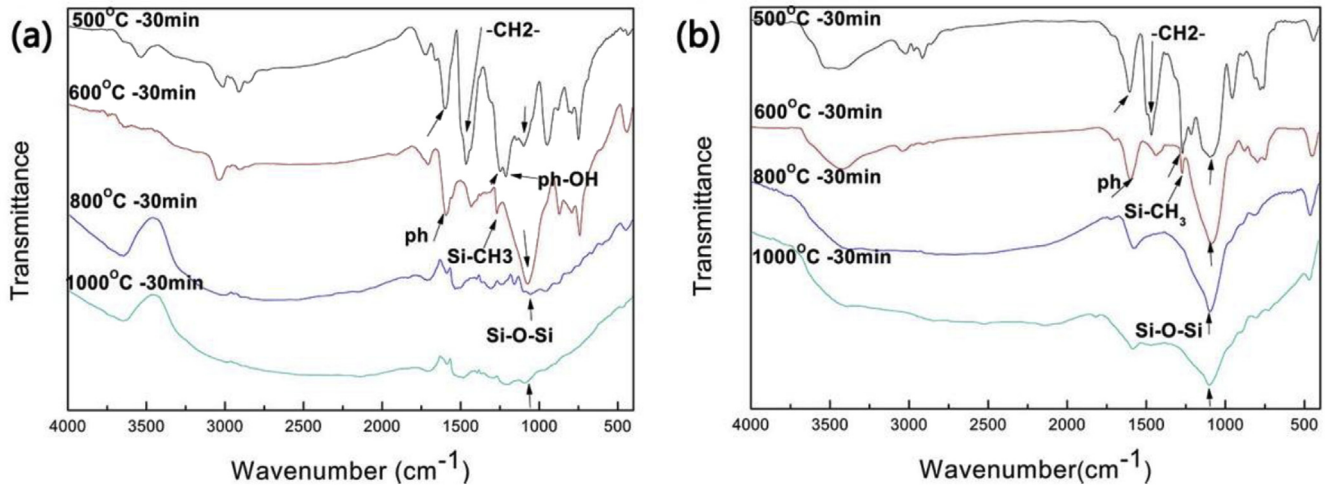

Fig. 9. FTIR spectra for the (a) cured SN, (b) cure SN-6%H_2O treating at different temperatures for 30 min in muffle furnace.

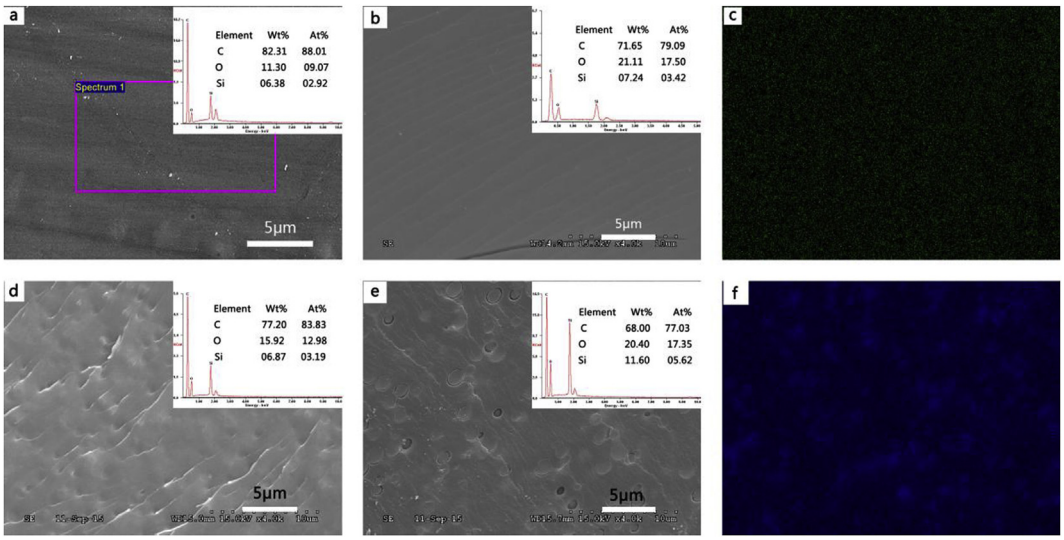

Fig. 10. SEM and EDX of (a) cured SN, (b) SN oxidized at 1000 °C for 30 min, (c) mapping of image "b"; (d) cured SN-10%H_2O, (e) SN-6%H_2O oxidized at 1000 °C for 30 min, (f) mapping of image "e".

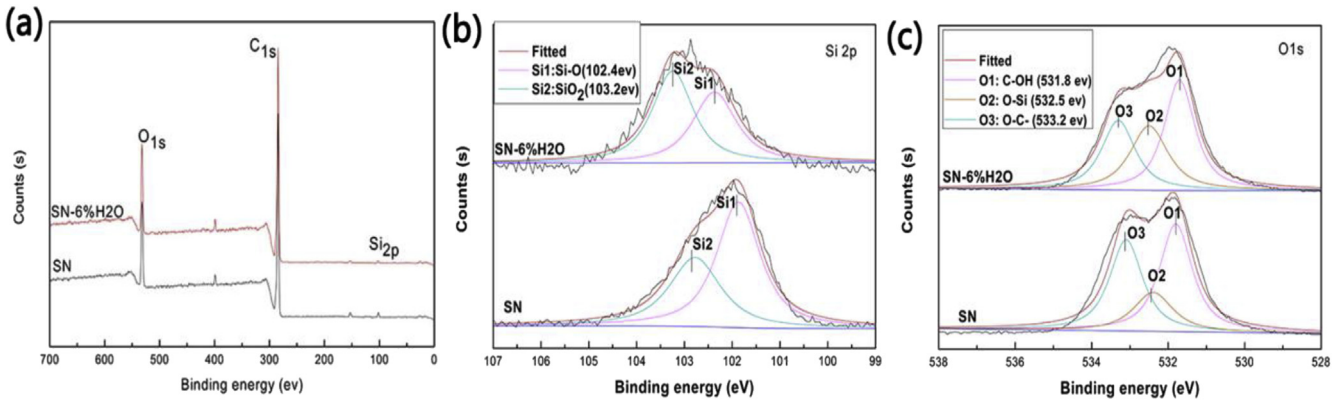

Fig. 11. X-ray photoelectron spectra of the SN and SN-6%H_2O after oxidized at 1000 °C for 30 min: (a) full scan, (b) high resolution Si 2p, (c) O1s.

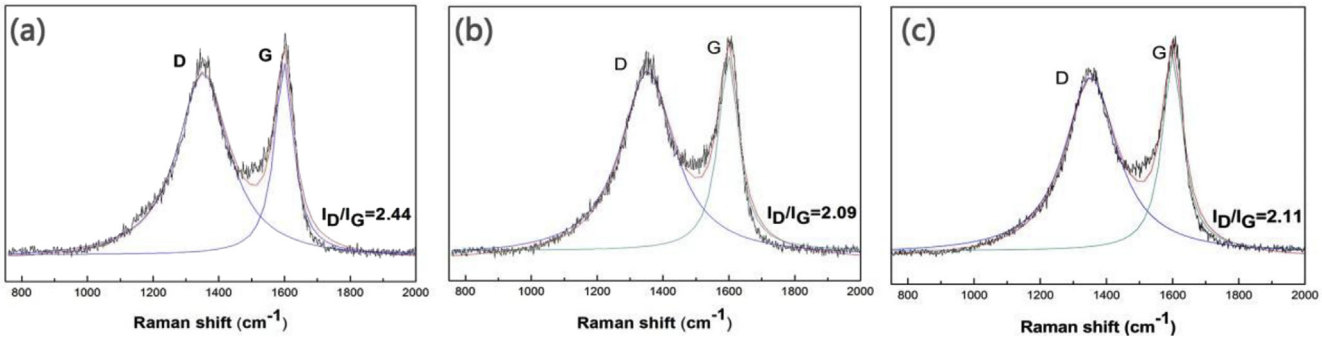

Fig. 12. Raman spectra and the I_D/I_G values of the hybrids (a) NR, (b) SN, (c) SN-6%H_2O after oxidation at 1000 °C for 30 min.

resulting in the loss of the silicon element during oxidation. The silane in SN-2%H_2O was also incompletely hydrolyzed and cured, thus the silicone rich domains would decompose during oxidation, generating many small holes in the silicone rich domains of the oxidized sample (as shown in Fig. 8b), and the decomposition rate was high. In SN-6%H_2O, the silane groups were either grafted on the phenolic resin or self-polymerized into silicone-rich domains. The grafted part of the silane could protect the phenol groups from oxidation; while the other part was higher in T_3 structure (as illustrated in Fig. 4), and would transform into void-free SiO_2-rich structures. These two aspects both contributed to the relatively higher R_{900} in air and higher silicone content of oxidized SN-6%H_2O, when compared with those of SN. The developed interface in SN-10%H_2O, resulting from the lack of chemical bond between the two components, would act as gas channel for oxygen permeation and lead to reduced oxidation resistance [24].

4. Conclusion

SN was successfully synthesized via esterification reaction between novolac resin and methyltrimethoxysilane, and hydrolyzation reaction was proceeded to control the degree of self-polymerization of silane in the hybrid. With water content increasing, more Si–O–ph bond was broken; while more Si–OCH_3 hydrolyzed and polycondensed, in-situ forming larger silicone-rich domains in the hybrid resin. Hybrid resins exhibited better thermal stability than the pure phenolic resin. The oxidation mechanism of the homogenous SN and phase separated SN-6%H_2O was compared. For SN, the silane grafted on the phenolic hydroxyl groups could protect phenolic hydroxyl groups from oxidation, but it would significantly loss during carbonization. In SN-6%H_2O, the silane groups were either grafted on the phenolic resin which could protect the phenol groups from oxidation, or self-polymerized into silicone-rich domains which would be oxidized into SiO_2-rich structures, resulting in the higher oxidation resistance.

These results provided useful clues for understanding the effects of structure on the thermal stability of silicone phenolic resin, which can be applied to the design of the anti-oxidation resins.

Acknowledgment

The authors gratefully acknowledge the financial support of the National Natural Science Foundation of China (No. 51473171 & No. 51403218).

References

[1] J. Gao, X. Li, W. Wu, H. Lin, Octa(aminophenyl) polyhedral oligomeric silsesquioxane/boron-containing phenol-formaldehyde resin nanocomposites: synthesis, cured, and thermal properties, Polym. Compos 32 (2011) 829–836.
[2] Y. Zhang, S. Shen, Y. Liu, The effect of titanium incorporation on the thermal stability of phenol-formaldehyde resin and its carbonization microstructure, Polym. Degrad. Stab. 98 (2013) 514–518.
[3] Y. Badhe, K. Balasubramanian, Reticulated three-dimensional network ablative composites for heat shields in thermal protection systems, RSC Adv. 4 (2014) 43708–43719.
[4] P. Xu, X. Jing, Pyrolysis of hyperbranched polyborate modified phenolic resin, Polym. Eng. Sci. 50 (2010) 1382–1388.
[5] P. Xu, X. Jing, High carbon yield thermoset resin based on phenolic resin, hyperbranched polyborate, and paraformaldehyde, Polym. Adv. Technol. 22 (2011) 2592–2595.
[6] S. Wang, X. Jing, Y. Wang, J. Si, High char yield of aryl boron-containing phenolic resins: the effect of phenylboronic acid on the thermal stability and carbonization of phenolic resins, Polym. Degrad. Stab. 99 (2014) 1–11.
[7] D.-C. Wang, G.-W. Chang, Y. Chen, Preparation and thermal stability of boron-containing phenolic resin/clay nanocomposites, Polym. Degrad. Stab. 93 (2008) 125–133.
[8] C. Martín, J.C. Ronda, V. Cádiz, Boron-containing novolac resins as flame retardant materials, Polym. Degrad. Stab. 91 (2006) 747–754.
[9] J. Gao, L. Xia, Y. Liu, Structure of a boron-containing bisphenol-F formaldehyde resin and kinetics of its thermal degradation, Polym. Degrad. Stab. 83 (2004) 71–77.
[10] Z. Guo, H. Li, Z. Liu, T. Zhao, Preparation, characterization and thermal properties of titanium- and silicon-modified novolac resins, High. Perform. Polym. 25 (2012) 42–50.
[11] C.-L. Chiang, C.-C.M. Ma, Synthesis, characterization, thermal properties and flame retardance of novel phenolic resin/silica nanocomposites, Polym. Degrad. Stab. 83 (2004) 207–214.
[12] Y. Zhang, S. Lee, M. Yoonessi, K. Liang, C.U. Pittman, Phenolic resin–trisilanolphenyl polyhedral oligomeric silsesquioxane (POSS) hybrid nanocomposites: Structure and properties, Polymer 47 (2006) 2984–2996.
[13] D. Zhuo, A. Gu, G. Liang, Hu J-t, L. Yuan, X. Chen, Flame retardancy materials based on a novel fully end-capped hyperbranched polysiloxane and bismaleimide/diallylbisphenol A resin with simultaneously improved integrated performance, J. Mater. Chem. 21 (2011) 6584.
[14] Y. Zhang, C. Shang, X. Yang, X. Zhao, W. Huang, Morphology and properties of TGDDM/DDS epoxy systems toughened by amino-bearing phenyl silicone resins, J. Mater. Sci. 47 (2012) 4415–4427.
[15] A. Santiago, L. Martin, J.J. Iruin, M.J. Fernández-Berridi, A. González, L. Irusta, Microphase separation and hydrophobicity of urethane/siloxane copolymers with low siloxane content, Prog. Org. Coat. 77 (2014) 798–802.
[16] Y. Ni, S. Zheng, K. Nie, Morphology and thermal properties of inorganic–organic hybrids involving epoxy resin and polyhedral oligomeric silsesquioxanes, Polymer 45 (2004) 5557–5568.
[17] Q. Ren, H. Zou, M. Liang, The preparation and properties study of methoxy functionalized silicone-modified epoxy resins, J. Appl. Polym. Sci. 131 (2014) (n/a-n/a).
[18] Y. Liu, S. Zheng, Inorganic-organic nanocomposites of polybenzoxazine with octa(propylglycidyl ether) polyhedral oligomeric silsesquioxane, J. Polym. Sci. Part A Polym. Chem. 44 (2006) 1168–1181.
[19] N. Furukawa, M. Yuasa, Y. Kimura, Characterization of polysiloxane-block-polyimides with silicate group in the polysiloxane segments, Polymer 40 (1999) 1853–1862.
[20] H. Ardhyananta, M.H. Wahid, M. Sasaki, T. Agag, T. Kawauchi, H. Ismail, et al., Performance enhancement of polybenzoxazine by hybridization with polysiloxane, Polymer 49 (2008) 4585–4591.
[21] K. Haraguchi, Y. Usami, K. Yamamura, S. Matsumoto, Morphological investigation of hybrid materials composed of phenolic resin and silica prepared by in situ polymerization, Polymer 39 (1998) 6243–6250.
[22] K. Haraguchi, Y. Usami, Y. Ono, The preparation and characterization of hybrid materials composed of phenolic resin and silica, J. Mater. Sci. 33 (1998) 3337–3344 (1998).
[23] W. Li, F. Liu, L. Wei, T. Zhao, Synthesis, morphology and properties of polydimethylsiloxane-modified allylated novolac/4,4′-bismaleimidodiphenylmethane, Eur. Polym. J. 42 (2006) 580–592.
[24] S. Li, F. Chen, Y. Han, H. Zhou, H. Li, T. Zhao, Enhanced compatibility and morphology evolution of the hybrids involving phenolic resin and silicone intermediate, Mater. Chem. Phys. 165 (2015) 25–33.
[25] Y. Chen, C. Hong, P. Chen, The effects of zirconium diboride particles on the ablation performance of carbon–phenolic composites under an oxyacetylene flame, RSC Adv. 3 (2013) 13734–13739.
[26] J-s Meng, Z-s Ji, Effect of La_2O_3/CeO_2 particle size on high-temperature oxidation resistance of electrodeposited Ni–La_2O_3/CeO_2 composites, Trans. Nonferr. Metal. Soc. 24 (2014) 3571–3577.
[27] S. Wen, K. Li, Q. Song, Y. Shan, Y. Li, H. Li, et al., Enhancement of the oxidation resistance of C/C composites by depositing SiC nanowires onto carbon fibers by electrophoretic deposition, J. Alloys Compd. 618 (2015) 336–342.
[28] C.-C.M. Ma, J.-M. Lin, W.-C. Chang, T.-H. Ko, Carbon/carbon nanocomposites derived from phenolic resin–silica hybrid ceramers: microstructure, physical and morphological properties, Carbon 40 (2002) 977–984.
[29] C. Li, K. Li, H. Li, Y. Zhang, H. Ouyang, D. Yao, et al., Microstructure and ablation resistance of carbon/carbon composites with a zirconium carbide rich surface layer, Corros. Sci. 85 (2014) 160–166.
[30] H. Li, D. Yao, Q. Fu, L. Liu, Y. Zhang, X. Yao, et al., Anti-oxidation and ablation properties of carbon/carbon composites infiltrated by hafnium boride, Carbon 52 (2013) 418–426.
[31] Y. Huang, J. Huang, L. Cao, C. Li, W. Hao, K. Zhu, Influence of solvothermal treatment time on oxidation of carbon/carbon composites containing ZrB2 micro-particles, Ceram. Int. 40 (2014) 13529–13535.
[32] J. Wang, N. Jiang, H. Jiang, Micro-structural evolution of phenol-formaldehyde resin modified by boron carbide at elevated temperatures, Mater. Chem. Phys. 120 (2010) 187–192.
[33] S. Sobhani, A. Jannesari, S. Bastani, Effect of molecular weight and content of PDMS on morphology and properties of silicone-modified epoxy resin, J. Appl. Polym. Sci. 123 (2012) 162–178.
[34] Kane, Phenolic resin compositions with improved impact resistance, United States Patent 5736619 (1998).
[35] C.-L. Chiang, C.-C.M. Ma, D.-L. Wu, H.-C. Kuan, Preparation, characterization, and properties of novolac-type phenolic/SiO2 hybrid organic-inorganic nanocomposite materials by sol-gel method, J. Polym. Sci. Part A Polym. Chem. 41 (2003) 905–913.
[36] M.R. Schütz, K. Sattler, S. Deeken, O. Klein, V. Adasch, C.H. Liebscher, et al., Improvement of thermal and mechanical properties of a phenolic resin nanocomposite byin situformation of silsesquioxanes from a molecular precursor, J. Appl. Polym. Sci. 117 (2010) 2272–2277.
[37] X. Sun, Y. Xu, D. Jiang, D. Yang, D. Wu, Y. Sun, et al., Study on the ammonia-catalyzed hydrolysis kinetics of single phenyltriethoxysilane and mixed phenyltriethoxysilane/tetraethoxysilane systems by liquid-state 29Si NMR, Colloids Surf. Physicochem. Eng. Asp. 289 (2006) 149–157.
[38] Y.-J. Lee, J.-M. Huang, S.-W. Kuo, J.-K. Chen, F.-C. Chang, Synthesis and characterizations of a vinyl-terminated benzoxazine monomer and its blending with polyhedral oligomeric silsesquioxane (POSS), Polymer 46 (2005) 2320–2330.
[39] S. Wang, Y. Wang, C. Bian, Y. Zhong, X. Jing, The thermal stability and pyrolysis mechanism of boron-containing phenolic resins: the effect of phenyl borates on the char formation, Appl. Surf. Sci. 331 (2015) 519–529.
[40] T.-H. Ko, W.-S. Kuo, Y.-H. Chang, Microstructural changes of phenolic resin during pyrolysis, J. Appl. Polym. Sci. 81 (2001) 1084–1089.
[41] X. Mao, F. Simeon, G.C. Rutledge, T.A. Hatton, Electrospun carbon nanofiber webs with controlled density of states for sensor applications, Adv. Mater 25 (2013) 1309–1314.
[42] J. Si, J. Li, S. Wang, Y. Li, X. Jing, Enhanced thermal resistance of phenolic resin composites at low loading of graphene oxide, Compos. Part A Appl. Sci. Manuf. 54 (2013) 166–172.